Available online at www.sciencedirect.com
ScienceDirect
Journal of Theoretical Biology 250 (2008) 172–185
Journal of Theoretical Biology
www.elsevier.com/locate/yjtbi

Origins of blood volume change due to glutamatergic synaptic activity at astrocytes abutting on arteriolar smooth muscle cells

M.R. Bennett[a,b,*], L. Farnell[b,c], W.G. Gibson[b,c]

[a]The Neurobiology Laboratory, Department of Physiology, University of Sydney, NSW 2006, Australia
[b]The Centre for Mathematical Biology, University of Sydney, NSW 2006, Australia
[c]The School of Mathematics and Statistics, University of Sydney, NSW 2006, Australia

Received 30 May 2007; received in revised form 20 August 2007; accepted 27 August 2007
Available online 1 September 2007

Abstract

The cellular mechanisms that couple activity of glutamatergic synapses with changes in blood flow, measured by a variety of techniques including the BOLD signal, have not previously been modelled. Here we provide such a model, that successfully accounts for the main observed changes in blood flow in both visual cortex and somatosensory cortex following their stimulation by high-contrast drifting grating or by single whisker stimulation, respectively. Coupling from glutamatergic synapses to smooth muscle cells of arterioles is effected by astrocytes releasing epoxyeicosatrienoic acids (EETs) onto them, following glutamate stimulation of the astrocyte. Coupling of EETs to the smooth muscle of arterioles is by means of potassium channels in their membranes, leading to hyperpolarization, relaxation and hence an increase in blood flow. This model predicts a linear increase in blood flow with increasing numbers of activated astrocytes, but a non-linear increase with increasing glutamate release.

Keywords: Blood volume; Astrocytes; Calcium waves

1. Introduction

Functional magnetic resonance imaging (fMRI) measures changes in the paramagnetic contrast agent deoxygenated hemoglobin in the vasculature and these are used to estimate changes in the electrical activity of neural networks associated with that vasculature. Blood oxygenation level-dependent (BOLD) signals are dependent on blood volume, blood flow and oxygen consumption. A large body of theoretical work has been concerned with developing quantitative descriptions of how these changes in the volume, flow and composition give rise to the BOLD signal (e.g., Jones et al., 2001; Zheng et al., 2002; Buxton and Frank, 1997; Buxton et al., 1998; Hoge et al., 1999) and how this signal is coupled to electrical activity in neural networks (e.g., Aubert and Costalat, 2002; Anderson and Nedergaard, 2003; Haydon and Carmignoto, 2006), a subject on which there is considerable controversy (e.g., Devor et al., 2005).

Grinvald and his colleagues have introduced optical microscopy techniques that allow for the measurement of the different components of the BOLD signal (Malonek et al., 1997; Malonek and Grinvald, 1996). They established that illumination of the surface of the cortex at 570 nm allowed imaging of activity-dependent blood volume increases whereas at 600–630 nm the signal is mostly due to activity-dependent oxygen delivery, with the latter occurring before the former (Frostig et al., 1990). Subsequent research has shown a close correlation between the functionally responsive area and the microvascular capillary beds (Harrison et al., 2002). In this work we consider how the cellular elements that constitute the arteriolar component of this vascular module, namely neurons and their synapses together with astrocytes and smooth muscle cells, interact to give rise to the blood volume changes in the arterioles that are detected by optical microscopy techniques at about 570 nm (Nemoto et al., 2004; Sheth et al., 2004; Vanzetta et al., 2005).

*Corresponding author. The Neurobiology Laboratory, Department of Physiology, University of Sydney, NSW 2006, Australia.
E-mail address: maxb@physiol.usyd.edu.au (M.R. Bennett).

0022-5193/$ - see front matter © 2007 Elsevier Ltd. All rights reserved.
doi:10.1016/j.jtbi.2007.08.024

Recent observations have shown that astrocytes play an intrinsic role in the functioning of neural networks (which should more accurately be called glial-neural networks), detecting local glutamatergic synaptic transmission (Dani et al., 1992) and thus providing coupling between glutamatergic synaptic activity in the vicinity of the arterioles and blood volume changes in the vascular module. In the present model, we show that astrocytic release of epoxyeicosatrienoic acids (EETs), triggered by the synaptic release of glutamate, can account for observations on the coupling of excitatory synaptic activity and blood volume changes in the vascular modules.

2. Theory

2.1. Spatial relationships between synapses, astrocytes, capillaries and arterioles in the model

Abutting on arterioles are the endfeet of astrocytes that form a sheath around vessels (Ramón y Cajal, 1995; Magistretti and Pellerin, 1996). Other processes of the astrocytes are in intimate contact with synapses, all of which are partly enclosed (except for their presynaptic membranes) by astrocyte processes. The model we have used to describe blood volume changes in the microcirculation, as a consequence of excitatory action at glutamate synapses, is depicted schematically in Fig. 1A. Glutamate is released from excitatory synapses onto astrocytes that are thus triggered to give a calcium transient which generates EETs that activate IK_{Ca} and IK_{ATP} channels in the smooth muscle cells of the adjacent arterioles, leading to their hyperpolarization, relaxation, and consequent increase in blood volume.

2.2. Overview of the model

The model covers the steps leading from the release of glutamate at synapses due to neural activity to the dilation of an arteriole following a reduction in cytosolic Ca^{2+} concentration ($[Ca^{2+}]$): (1) neural activity leads to glutamate release at synapses; (2) glutamate overspill acts on metabotropic receptors on astrocyte processes surrounding these synapses, leading to the production and release of EETs from the astrocytes, and particularly from their endfeet; (3) the EETs diffuse to hyperpolarize the smooth muscle cells of the arteriole; (4) this hyperpolarization propagates electronically along the smooth muscle cells of the arteriole; (5) this leads to the closure of L-type Ca^{2+} channels and the subsequent decrease in cytosolic $[Ca^{2+}]$ results in vasodilation and hence increased blood flow.

The cell types involved in the model are astrocytes and smooth muscle cells. In the astrocytes, receptor activation initiates a *G*-protein cascade, leading to the production of inositol trisphosphate (IP_3) and the subsequent release of Ca^{2+} from internal stores and then EETs from the astrocyte (Fig. 1B(a)). An astrocyte is treated as a single well-mixed cubic compartment of side 25 μm (Fig. 1C); thus, no allowance has been made for the time course of Ca^{2+} wave propagation in the astrocyte which might be of the order of 1 s or so (see Fig. 1 in Filosa et al., 2004). However, such a delay can be compensated for by speeding up the actin–myosin system within the smooth muscle. In the smooth muscle cells, these EETs cause a hyperpolarization leading to the closure of L-type Ca^{2+} channels and subsequent relaxation of the contractile machinery (Fig. 1B(b)). The equations describing the internal processes in each cell type are as follows.

2.3. Astrocyte

The single-cell model follows that of Bennett et al. (2005b) which in turn is based on Lemon et al. (2003) (Fig. 1B(a)).

Receptor binding is reversible, according to

$$L + R \underset{k_1^-}{\overset{k_1^+}{\rightleftarrows}} LR, \tag{1}$$

where L is ligand and R receptor. The quantity we want is the ratio of bound to total receptors, $\rho = [LR]/[R_T]$, where $[R_T] = [R] + [LR]$ is the total number of receptors. Under the assumption of fast binding kinetics Eq. (1) can be assumed to be in equilibrium, leading to

$$\rho = \frac{[Glu]}{K_{Glu} + [Glu]}, \tag{2}$$

where $[L] = [Glu]$ is the extracellular glutamate concentration and $K_{Glu} = k_1^-/k_1^+$ is the dissociation constant.

The reaction describing *G*-protein activation is (Eq. (4) in Bennett et al., 2005b)

$$G_{in} \underset{k_d}{\overset{k_a(\rho+\delta)}{\rightleftarrows}} G, \tag{3}$$

where G is active *G*-protein and G_{in} is inactive *G*-protein, so $[G_{in}] = [G_T] - [G]$ where $[G_T]$ is total *G*-protein; ρ is the fraction of bound receptors as given by Eq. (2), δ is the ratio of the activities of the unbound and bound receptors (and thus allows for background activity even in the absence of ligand binding, that is, unbound receptors can activate a small amount of *G*-protein), and k_a and k_d are the *G*-protein activation and deactivation rate parameters, respectively. Again assuming fast kinetics, we obtain

$$G^* = \frac{\rho + \delta}{K_G + \delta + \rho}, \tag{4}$$

where $G^* = [G]/[G_T]$ and $K_G = k_d/k_a$.

IP_3 production, diffusion and degradation is governed by (Eq. (8) in Bennett et al., 2005b)

$$\frac{\partial [IP_3]}{\partial t} = r_h^* G^* + D_{IP}\nabla^2[IP_3] - k_{deg}[IP_3], \tag{5}$$

where r_h^* and k_{deg} are constants, G^* is given by (4) and D_{IP} is the diffusion coefficient for IP_3. The term $r_h^* G^*$ is applied only at the cell wall. In deriving this equation it has been

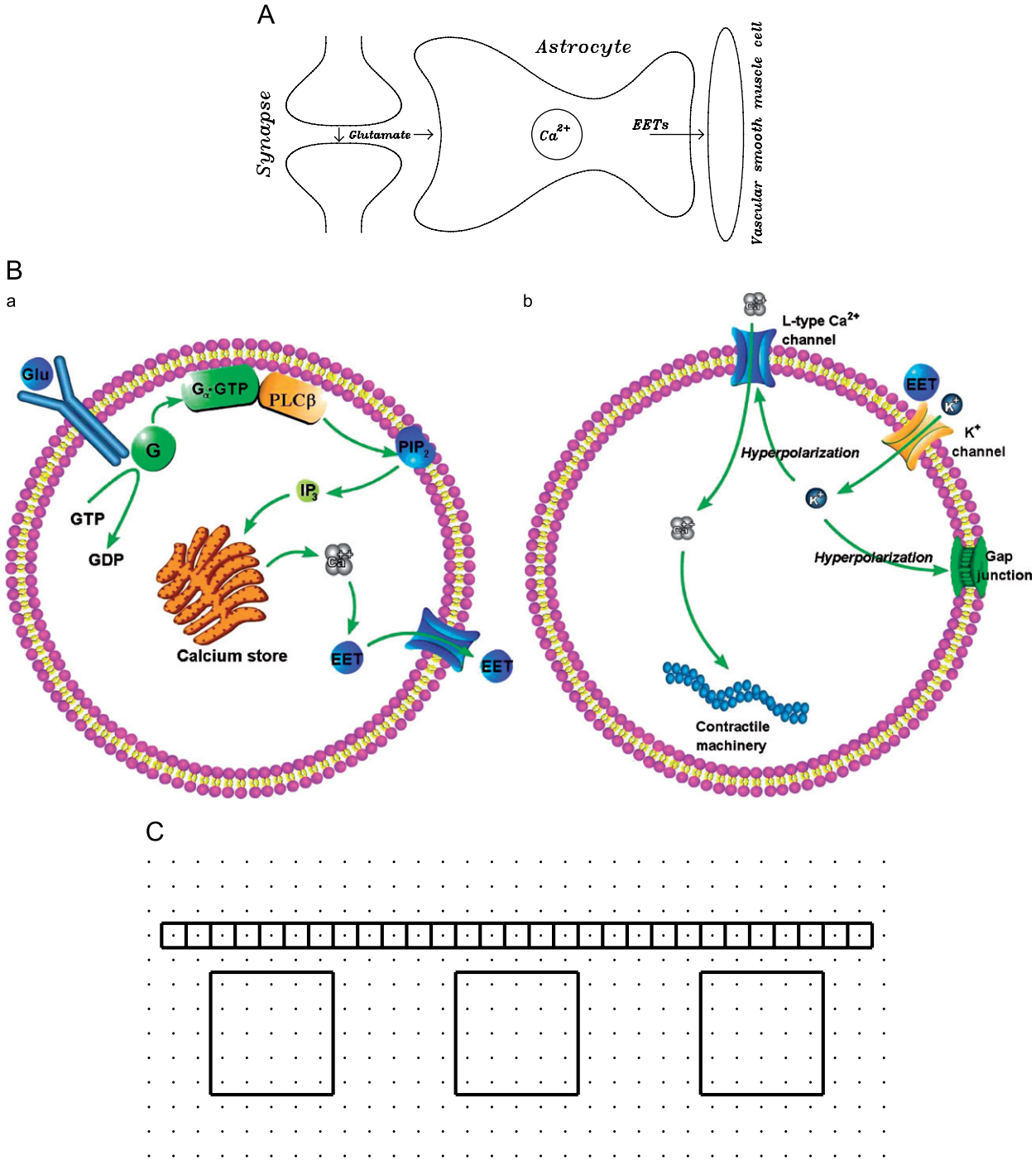

Fig. 1. (A) schematic overview of the model. Glutamate released from the presynaptic terminal of a neuron acts on metabotropic receptors on the astrocyte processes, leading to the release of Ca^{2+} from internal stores and the subsequent efflux of EETs from the astrocyte, where they act to hyperpolarize the smooth muscle cells, leading to vascular dilation. (Cf. Harder et al., 2000, Fig. 1; Anderson and Nedergaard, 2003, Fig. 1(b); Haydon and Carmignoto, 2006, Fig. 1; Koehler et al., 2006, Fig. 3.) (B) Schematic diagram of the cell types used in the model, indicating the various internal processes that occur: (a) astrocyte, (b) smooth muscle cell. (C) Geometric structure of the model. The astrocytes are represented by cubes of side 25 μm cf. (Bennett et al., 2005b), and the smooth muscle cells as elongated tubes with square cross section of 5 μm. The endfeet of astrocytes are about 10–20 μm long (see Fig. 5 in Straub et al., 2006 and Fig. 1A in Filosa et al., 2004) and cover a portion of about one to two smooth muscle cells (diameter about 5 μm) which wrap twice around an arteriole of 14 μm diameter (see Figs. 2 and 3A in Seidel et al., 1991); several end-feet are therefore present at any arteriolar cross-section. The diagram shows a cross-sectional view of these cells, together with the grid points, spacing 5 μm (in all three dimensions), used in the numerical calculations.

assumed that there is no depletion of PIP_2 and also the catalytic effect of Ca^{2+} on IP_3 production has been neglected.

The steps leading from IP_3 production to Ca^{2+} release from the ER are based on the theories of De Young and Keizer (1992) and Li and Rinzel (1994), as modified by

Fink et al. (1999). The Ca^{2+} dynamics are governed by

$$\frac{d[Ca^{2+}]}{dt} = \beta_{cyt}(J_{IP_3} - J_{pump} + J_{leak}), \quad (6)$$

where $[Ca^{2+}]$ is the cytosolic Ca^{2+} concentration, J_{IP_3}, J_{pump} and J_{leak} are the rates of Ca^{2+} concentration change due to release through IP_3R channels, pump uptake into the ER, and leak from the ER, respectively, and β is a factor describing Ca^{2+} buffering. The IP_3-induced current is

$$J_{IP_3} = J_{max}\left[\left(\frac{[IP_3]}{[IP_3]+K_I}\right)\left(\frac{[Ca^{2+}]}{[Ca^{2+}]+K_{act}}\right)h\right]^3 \times\left[1-\frac{[Ca^{2+}]}{[Ca^{2+}]_{ER}}\right], \quad (7)$$

where J_{max} is the maximum rate, K_I is the dissociation constant for IP_3 binding to an IP_3R, K_{act} is the dissociation constant for Ca^{2+} binding to an activation site on an IP_3R, $[Ca^{2+}]_{ER}$ is the Ca^{2+} concentration in the ER (taken to be constant) and h satisfies

$$\frac{dh}{dt} = k_{on}[K_{inh} - ([Ca^{2+}] + K_{inh})h], \quad (8)$$

where k_{on} is the rate of Ca^{2+} binding to the inhibitory site on the IP_3R and K_{inh} is the corresponding dissociation constant. The ATPase Ca^{2+} pump is described by

$$J_{pump} = V_{max}\frac{[Ca^{2+}]^2}{[Ca^{2+}]^2 + K_p^2}, \quad (9)$$

where V_{max} is the maximum pumping rate and K_p is the dissociation constant. The leak is described by

$$J_{leak} = P_L\left(1 - \frac{[Ca^{2+}]}{[Ca^{2+}]_{ER}}\right), \quad (10)$$

where the constant P_L is determined by steady-state flux balance. The buffering is described by the steady-state approximation

$$\beta_{cyt} = \left(1 + \frac{[B]_{end}}{K_{end}}\right)^{-1}, \quad (11)$$

where $[B]_{end}$ and K_{end} are the concentration and dissociation constants of the endogenous buffer.

The production and diffusion of EETs is governed by

$$\frac{d[EET]}{dt} = V_{EET}([Ca^{2+}] - [Ca^{2+}]_{min}) + D_{EET}\nabla^2[EET], \quad (12)$$

where D_{EET} is the diffusion coefficient for EET and V_{EET} is a constant and $[Ca^{2+}]_{min}$ is the minimum $[Ca^{2+}]$ for EET production. The EET clearance, either by uptake into the phospholipid pool or by metabolism by epoxide hydrolase, depends on the concentration of EET, so that changes in uptake/metabolism are approximately equivalent to changes in release, and hence no such mechanisms have been explicitly included in Eq. (12).

We do not include ATP-dependent transmission of Ca^{2+} waves between adjoining astrocytes (see Bennett et al., 2006) since a recent paper (Straub et al., 2006) shows that stimulation of neurons can give rise to Ca^{2+} transients in single endfeet, implying little propagation of Ca^{2+} waves between the endfeet.

Owing to the paucity of quantitative information concerning the kinetics of a number of processes involving the release and metabolism of EETs we have not modelled each of these, but rather give an overall transfer function for its release (Eq. (12)). Aspects not modelled explicitly include: (1) the relation between Ca^{2+} and phospholipase activity; (2) the kinetics of epoxygenase activity for *de novo* EETs synthesis; (3) the release of preformed EETs from the phospholipid pool as a function of Ca^{2+}; (4) the reuptake kinetics of EETs into the phospholipid pool and (5), the kinetics of epoxide hydrolase metabolisms. More complicated dependencies on $[Ca^{2+}]$ were also tried, but it was found that the agreement with experiment was no better than that obtained using the simple linear dependence given in Eq. (12).

2.4. Smooth muscle cell

EETs act on a smooth muscle cell to cause a hyperpolarization according to

$$\frac{dV_m}{dt} = -\gamma_{EET}[EET], \quad (13)$$

where γ_{EET} is a constant. This hyperpolarization closes L-type Ca^{2+} channels in the plasmalemma, thus preventing the influx of Ca^{2+} into the cytosol (Fig. 1B(b)). The open probability of a single channel is

$$p = \frac{1}{1 + \exp[(V_h - V_m)/k]}, \quad (14)$$

where V_h and k are constants and V_m (mV) is the membrane potential; the single-channel current is

$$i_{Ca} = \kappa\frac{V_m - \overline{V}}{1 - \exp[0.075(V_m - \overline{V})]}, \quad (15)$$

where κ and $\overline{V}$ are constants (Rubart et al., 1996). The whole-cell current through the L-type Ca^{2+} channels is thus $I_{Ca} = Npi_{Ca}$ where N is the total number of L-type Ca^{2+} channels on a smooth muscle cell. The Ca^{2+} concentration in a smooth muscle cell is then governed by

$$\frac{d[Ca^{2+}]}{dt} = \alpha I_{Ca} - \beta([Ca^{2+}] - [Ca^{2+}]_0), \quad (16)$$

where $[Ca^{2+}]_0$ is the background $[Ca^{2+}]$ and α and β are constants. The assumption of fast equilibrium leads to

$$[Ca^{2+}] = [Ca^{2+}]_0 + \frac{[Ca^{2+}](t=0) - [Ca^{2+}]_0}{I_{Ca}(t=0)}I_{Ca}, \quad (17)$$

where $[Ca^{2+}](t=0) \equiv [Ca^{2+}]_{init}$ is the initial $[Ca^{2+}]$ and $I_{Ca}(t=0)$ is the corresponding current.

The smooth muscle cells are connected by gap junctions. If R_i is the effective resistance between two smooth muscle cells, being the sum of the gap-junction resistance plus cytosolic resistance, the membrane potential of the jth cell, V_m^j, is governed by the usual cable equation

$$C_m \frac{dV_i^j}{dt} = \frac{V_0 - V_i^j}{R_m} + \frac{V_i^{j+1} - 2V_i^j + V_i^{j-1}}{R_i}, \quad (18)$$

where C_m and R_m are the membrane capacitance and resistance, respectively. Contraction in a smooth muscle cell is triggered by a rise in cytosolic Ca^{2+} leading to a chain of events that starts with Ca^{2+} binding to calmodulin (and thus a decrease in $[Ca^{2+}]$ as a result of the closing of L-type Ca^{2+} channels will lead to relaxation of the muscle cells). This activates myosin light chain kinase which then catalyses the phosphorylation of myosin II and the interaction of phosphorylated myosin II with actin leads to contraction. We use a simple model for the interaction (Hai and Murphy, 1988; Bennett et al., 2005a):

$$M \underset{k_2}{\overset{k_1}{\rightleftarrows}} M_P \underset{k_4}{\overset{k_3}{\rightleftarrows}} AM_P, \quad (19)$$

where M denotes myosin, M_P phosphorylated myosin and A actin. The k_i's, $i = 1, \ldots, 4$, are rate coefficients, where k_2, k_3, k_4 are constants and k_1 depends on cytosolic calcium concentration, $[Ca^{2+}]_i$. Specifically, $k_1 = k_m([Ca^{2+}]_i)^n$ where k_m and n are constants. The contractile force is proportional to the concentration of actin bound to phosphorylated myosin, $[AM_P]$. From Eq. (19), the equations governing the concentrations are

$$\frac{d[M]}{dt} = k_2([M_T] - [AM_P]) - (k_1 + k_2)[M], \quad (20)$$

$$\frac{d[AM_P]}{dt} = k_3([M_T] - [M]) - (k_3 + k_4)[AM_P], \quad (21)$$

where $[M_T] = [M] + [M_P] + [AM_P]$ is the total concentration of myosin, taken to be 1 (arbitrary units). The contraction of the muscle cell is taken to be proportional to $[AM_P]$. The change in cell length is translated into a change in arteriole diameter and hence by integration to a change in blood volume (cf. Tyml et al., 2003).

2.5. Numerical scheme

The numerical scheme is implemented on a three-dimensional spatial grid, a two-dimensional section of which is shown in Fig. 1C, where a representative number of grid points are shown as dots. The diffusion equations are solved using a "leap-frog" method and the other differential equations using a standard Runge–Kutta method; further details are in Bennett et al. (2005b).

2.6. Parameter choice

The parameter values used in the calculations are listed in Table 1. For astrocytes, the values are mostly those used in our previous model of these cells (Bennett et al., 2005b). The maximum pumping rate for Ca^{2+} into the ER, V_{max}, was increased to give a faster timecourse of Ca^{2+} clearance from the astrocyte cytosol. Because of IP_3 diffusion inside cells, the initial background level was spatially inhomogeneous and had to be set by running the program to a steady state (see "Initialization" in Bennett et al., 2005b); this background level must then be used when setting $[IP_3]_{min}$. The parameters for EET were set to values that gave final results in agreement with experiment. There was some flexibility here, in that changes in the production rate, determined by V_{EET} could be compensated for by changes in the conversion rate γ_{EET}. The contraction model for a smooth muscle cell follows that of Hai and Murphy (1988) and they give parameter values that were found to be appropriate for the rat tail artery (Bennett et al., 2005a). However, if arteriole dilation is to occur with the correct timescale it is necessary to change these parameter values to those given in Table 1.

2.7. Critical parameter values in the model for determining the timecourse and amplitude of the blood volume changes in response to synaptic activity

The time courses of $[IP_3]$ and $[Ca^{2+}]$ are mainly determined by equations and parameter values that we have used in previous work (Bennett et al., 2005b, 2006), although as noted above the pumping rate of Ca^{2+} into the ER has been increased. The main parameters that affect the time course of the arteriolar blood flow are those associated with the kinetic model of smooth muscle contraction, and these have been increased above those values used in a model of the rat tail artery (Bennett et al., 2005a) in order to get better agreement with experiment.

The amplitude of the blood volume change is affected by a number of parameters, including the initial glutamate release. In particular, it is affected by the parameters governing the production and effect of EETs. In the absence of detailed information on these processes, simple relations have been assumed (Eqs. (12) and (13)) and values for V_{EET} and γ_{EET} have been adjusted to give reasonable peak potential changes in the smooth muscle cells. More complicated equations were tried in place of Eqs. (12) and (13), but there was little qualitative change to the results.

3. Results

The IP_3 concentration ($[IP_3]$) in an astrocyte (Fig. 2B), generated by the action of a transient increase in glutamate acting on metabotropic receptors (Fig. 2A), increases for the duration of the 2 s glutamate transient; the $[IP_3]$ then declines to very low basal levels over the next 3 s (Fig. 2B). This IP_3 releases calcium from the endoplasmic reticulum of the astrocyte, with the $[Ca^{2+}]$ reaching a peak just before the peak of $[IP_3]$ (Fig. 2C) and then declining to the very low basal $[Ca^{2+}]$ of 50 nM in 3–4 s (Fig. 2C). At the same time, there is a second-messenger triggered release of EETs from the astrocyte, with the [EET] adjacent to the astrocyte

Table 1

Symbol	Definition	Value	Notes
Astrocyte			
G-protein cascade			
k_{deg}	IP_3 degradation rate	$1.25\,s^{-1}$	Lemon et al. (2003)
K_G	G-protein dissociation constant	8.82	Lemon et al. (2003)
r_h^*	IP_3 production rate	$2\times10^{-14}\mu mol\,\mu m^{-2}s^{-1}$	Bennett et al. (2005b)
D_{IP}	IP_3 diffusion coefficient	$280\,\mu m^2s^{-1}$	Bennett et al. (2005b)
Ca^{2+} dynamics			
J_{max}	Maximum channel current	$2880\,\mu M\,s^{-1}$	Fink et al. (1999)
K_I	IP_3 channel kinetic parameter	$0.03\,\mu M$	Fink et al. (1999)
K_{act}	IP_3 channel kinetic parameter	$0.17\,\mu M$	Fink et al. (1999)
k_{on}	IP_3 channelkinetic parameter	$2.0\,\mu M\,s^{-1}$	Bennett et al. (2005b)
K_{inh}	IP_3 channel kinetic parameter	$0.1\,\mu M$	Fink et al. (1999)
$[Ca^{2+}]_{ER}$	Ca^{2+}concentration in ER	$400\,\mu M$	Fink et al. (1999)
V_{max}	Maximum pumping rate into ER	$20\,\mu M\,s^{-1}$	See text
K_p	Pump dissociation constant	$0.24\,\mu M$	Fink et al. (1999)
β_{cyt}	Endogenous buffer parameter	0.0244	Fink et al. (1999)
Initial values			
$[IP_3]_0$	Initial IP_3 conc.	$0.01\,\mu M$	Lemon et al. (2003)
$[Ca^{2+}]_0$	Initial Ca^{2+} conc.	$0.05\,\mu M$	Fink et al. (1999)
EET			
D_{EET}	Diffusion coefficient	$500\,\mu m^2s^{-1}$	Estimate from molecular weight
V_{EET}	Production rate	$3\times10^{-13}\mu mol\,\mu m^{-2}s^{-1}$	See text
$[Ca^{2+}]_{min}$	Minimum $[Ca^{2+}]$ for production	$0.1\,\mu M$	See text
Smooth muscle cell			
Membrane potential			
γ_{EET}	EET conversion factor	$0.004\,V\,\mu M^{-1}s^{-1}$	See text
L-type Ca^{2+} channel			
V_h	Open probability parameter	6.2 mV	(Rubart et al., 1996)
k	Open probability parameter	9.5 mV	(Rubart et al., 1996)
κ	Single-channel current parameter	$4.1\,pA\,V^{-1}$	Fitted to Rubart et al. (1996)
$\overline{V}$	Single-channel current parameter	1.44 mV	Fitted to Rubart et al. (1996)
$[Ca^{2+}]_0$	Background $[Ca^{2+}]$	$0.05\,\mu M$	
$[Ca^{2+}]_{init}$	Initial $[Ca^{2+}]$	$0.3\,\mu M$	Estimate from experiment
Electrical			
R_i	Cytoplasmic resistance	$5\times10^7\,\Omega$	Bennett et al. (2001)
R_m	Membrane resistance	$3.6\times10^9\,\Omega$	Bennett et al. (2001)
C_m	Membrane capacitance	8.4×10^{-11} F	Bennett et al. (2001)
V_0	Initial membrane potential	−30 mV	Emerson et al. (2002)
Contraction			
k_m	Myosin phosphorylation rate	$80\,\mu M^{-4}s^{-1}$	See text
k_2	Myosin dephosphorylation rate	$20\,s^{-1}$	See text
k_3	Actin binding rate	$4\,s^{-1}$	See text
k_4	Actin unbinding rate	$1\,s^{-1}$	See text

rising to peak values by the end of the 2 s glutamate synapse activation period (Fig. 2D); this [EET] then declines to low levels over about the next 6 s (Fig. 2D).

The release of EETs onto the arteriolar smooth muscle sets in train the events leading to arteriole dilation. The first of these events is the activation of the I_K channels in the membrane of the smooth muscle cell adjacent to the astrocyte, leading to up to about a 4 mV hyperpolarization of the muscle cell (Fig. 3A, solid line). This hyperpolarization then propagates electrotonically along the smooth muscle syncytium (see Bennett, 1972), with decreasing amplitude (Fig. 3B). This drives different degrees of relaxation of the smooth muscle cells, highest nearest the point of astrocytic release of EETs and less further away

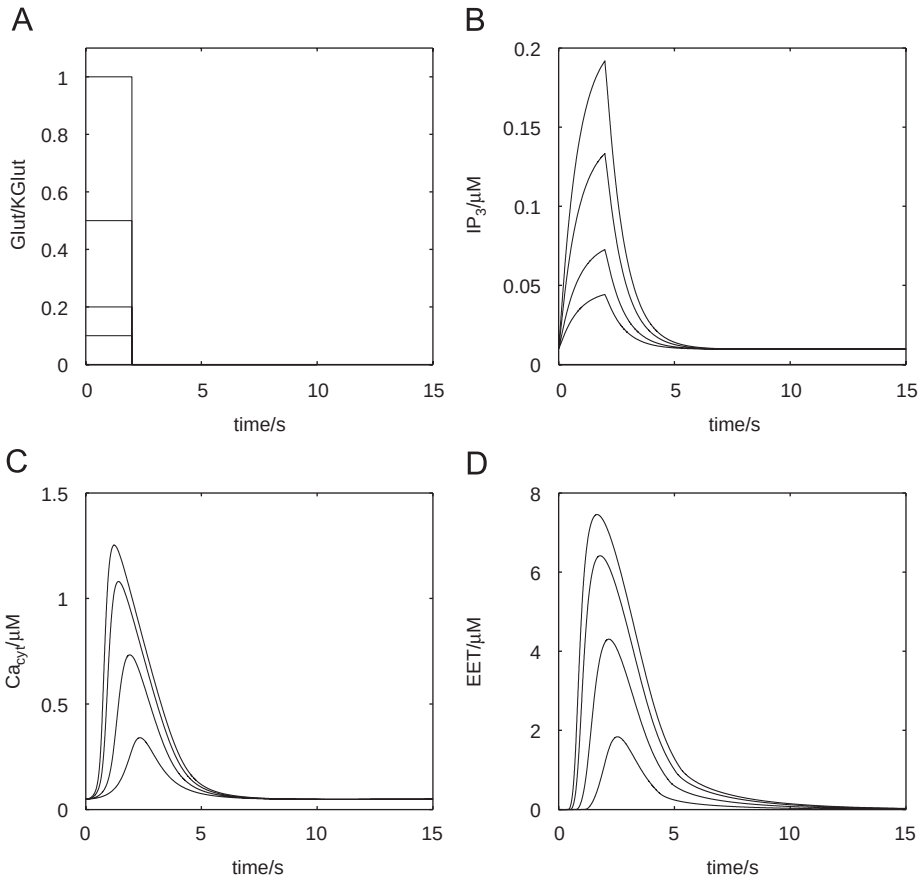

Fig. 2. Model changes in an astrocyte as a result of glutamate activation of metabotropic receptors on the astrocyte. (A) Step release of glutamate for 2 s. (B) Resulting intracellular [IP_3]. (C) Corresponding intracellular [Ca^{2+}] resulting from release from internal stores. (D) Resulting [EET] in the extracellular space, computed at a point between and astrocyte and a smooth muscle cell. Results are shown for the four different concentrations of glutamate given in A.

(Figs. 3C and D). The resulting dilation of the arteriole leads to an increase in blood flow and concomitantly of blood volume (Figs. 3E and F). Shown also in Fig. 3 are the results of increasing the coupling resistance between the smooth muscle cells from $R_i = 5 \times 10^5\,\Omega$ (dotted line) to $5 \times 10^7\,\Omega$ (solid line) to $5 \times 10^9\,\Omega$ (dashed line). This increase results in a localized large hyperpolarization of the smooth muscle cells at the site of the active astrocyte (Fig. 3B), accompanied by a large relaxation there (Figs. 3C and D) giving rise to a smaller change in blood flow and blood volume because of the restricted length of arteriole affected (Figs. 3E and F).

It is unlikely that only a single astrocyte abutting on an arteriole is activated during physiological activity. The effect on blood flow of simultaneous activation of three nearby astrocytes by glutamatergic synaptic activity is shown in Fig. 4. If there is a high resistance coupling between the smooth muscle cells ($R_i = 5 \times 10^9\,\Omega$) then discrete regions of the arteriolar smooth muscle are hyperpolarized, namely those beneath each astrocyte end-foot (Fig. 4B, dashed line). These are accompanied by discrete sites of relaxation along the arteriole (Figs. 4C and D, dashed lines), giving rise to changes in blood flow and blood volume substantially larger than those that occur in response to single astrocyte activation (compare Figs. 4E and F with Figs. 3C and D, respectively). Lower resistance coupling ($R_i = 5 \times 10^7\,\Omega$) between the smooth muscle cells smooths the hyperpolarization and relaxation of the arteriole but still leaves it relatively localized (Figs. 4B, C and D, solid lines), but gives rise to larger changes in blood flow and blood volume (Figs. 4E and F, solid lines). A further reduction to $R_i = 5 \times 10^5\,\Omega$ removes this localized response (Figs. 4B, C and D, dotted lines) and leads to even larger changes in blood flow and volume (4E and F, dotted lines).

A summary of the effects of exciting different numbers of adjacent astrocytes on arteriole volume is shown in Fig. 5A. There is a linear relationship between astrocyte number and changes in blood volume. However, increasing excitation with glutamate of a single astrocyte gave a non-linear increase in the blood volume (Fig. 5B). Thus either increased localized synaptic transmission or an increase in the number of astrocytes recruited during transmission increases blood volume, but increases in glutamatergic transmission give rise to proportionally smaller increases in blood volume.

In visual area 18 of anesthetized cats, optical imaging of intrinsic signals at a near-isosbestic wavelength for

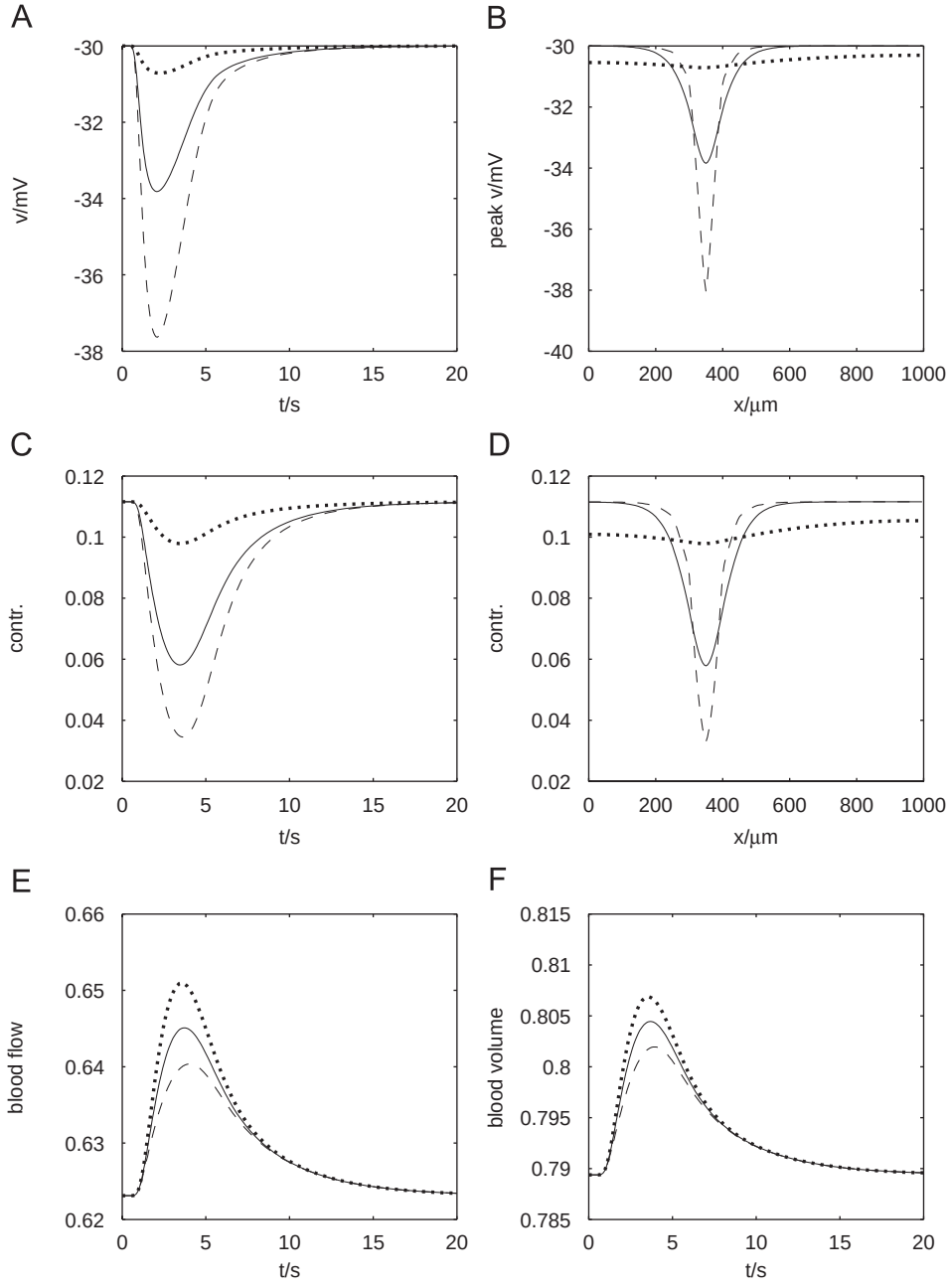

Fig. 3. Model changes in smooth muscle cells and arteriolar blood flow due to the action of glutamate released onto an astrocyte from synapses; the timecourse of release of EETs is as shown in Fig. 2D, top curve. (A) Time course of the membrane potential of smooth muscle cells due to the action of EETs in opening smooth-muscle IK channels. (B) Peak membrane potential, as a function of distance along the arteriole. (C) Time course of relaxation of the arteriole. (D) Peak relaxation as a function of distance along the arteriole. (E) Changes in blood flow. (F) Blood volume, as a result of the relaxation of the arteriolar smooth muscle. In each case, the three curves are for different couplings between the smooth muscle cells: $R_i = 5 \times 10^7\,\Omega$ (solid line); $R_i = 5 \times 10^9\,\Omega$ (dashed line); $R_i = 5 \times 10^5\,\Omega$ (dotted line).

hemoglobin (565 nm) during presentation of visual stimuli consisting of high-contrast full-field vertical and horizontal drifting square gratings, allows determination of the detailed spatio-temporal dynamics of blood volume changes in the various microvascular compartments (Vanzetta et al., 2005). The vascular response begins at the arteriolar level, spreading from there towards the capillaries and venules. The time course of the observed changes in blood volume in the arterioles during and after a 2 s period of visual stimulation is shown in Fig. 6A (solid line). This consists of a transient with a delay of about 0.8 s after first presentation of the visual stimulus, followed by a peak blood volume change at about 3.5 s, with a decline to 50% of the peak value in about a further 4 s. The model changes in blood volume in an arteriole under the conditions of glutamatergic input for 2 s onto a single astrocyte abutting onto the arteriole are also shown (dashed line), for comparison with the experimental results.

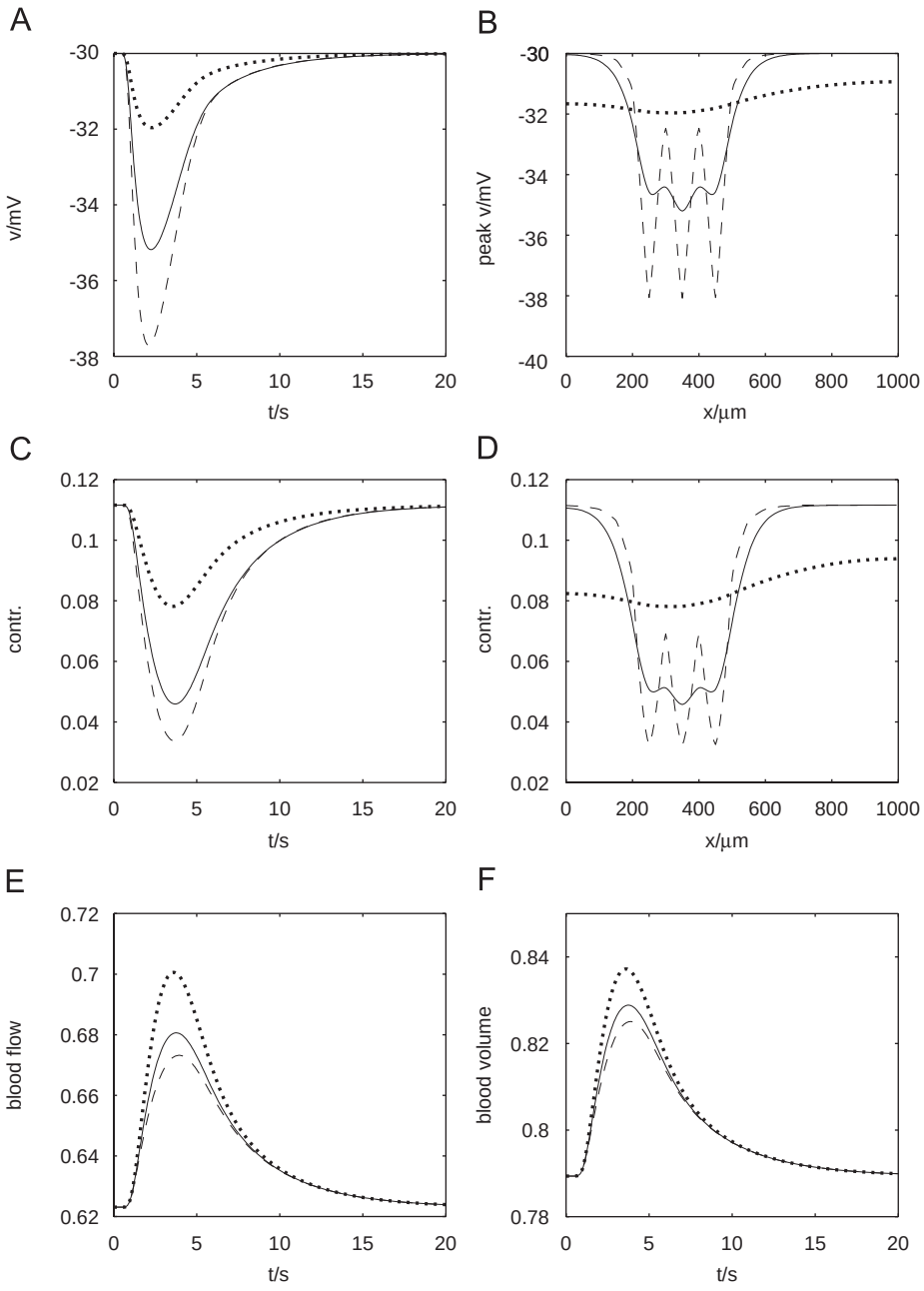

Fig. 4. Model changes in smooth muscle cells and arteriolar blood flow due to the action of glutamate released simultaneously onto three astrocytes with centres 100 μm apart. (A) Time course of the membrane potential of smooth muscle cells due to the action of EETs in opening smooth-muscle IK channels. (B) Peak membrane potential, as a function of distance along the arteriole. (C) Time course of relaxation of the arteriole. (D) Peak relaxation as a function of distance along the arteriole. (E) Changes in blood flow. (F) Blood volume, as a result of the relaxation of the arteriolar smooth muscle. In each case, the three curves are for different couplings between the smooth muscle cells, as for Fig. 3.

In this case, the model result is very similar to that observed experimentally.

Spatiotemporal characteristics of microvascular responses to neuronal activation in rat barrel cortex have also been determined using optical imaging of intrinsic signals at an isosbestic wavelength of hemoglobin (Sheth et al., 2004). Observation of the blood volume changes in the parenchyma of a stimulated barrel column in response to a whisker deflection over 2 s are shown in Fig. 6B (solid line). The transient blood volume changes have only a short delay after the beginning of whisker deflection, followed by a peak volume change at about 2.8 s, with a decline to 50% in a further 2 s. This response therefore rises to a peak value about 1 s earlier than the blood volume changes in the capillaries of area 18 following the beginning of visual stimuli, but declines more rapidly (compare Fig. 6B with 6A). Clearly, the experimental result shown in Fig. 6B is quantitatively incompatible with that of Fig. 6A and hence the theoretical curve in Fig. 6B (dashed line) is not in good agreement. Better agreement can be obtained

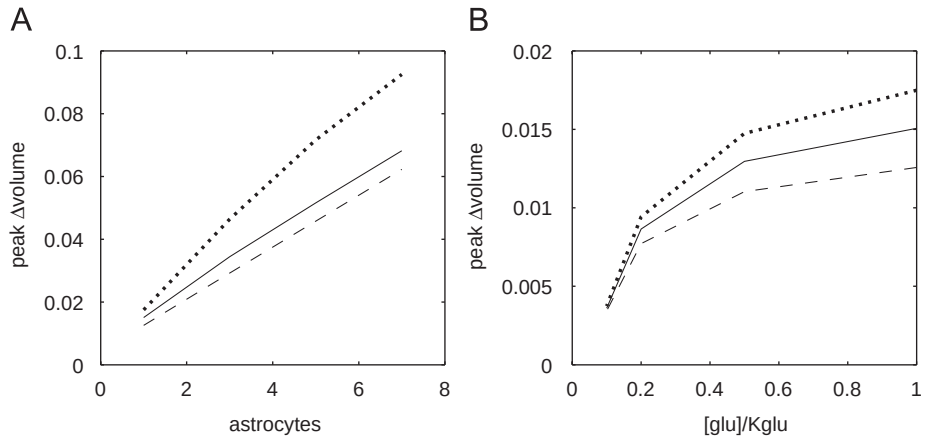

Fig. 5. The effect of glutamatergic transmission on blood volume. (A) The effect of increasing the number of adjacent astrocytes activated by a fixed amount of glutamate on blood volume changes. (B) The effect of increasing the amount of glutamate released onto an astrocyte during 2 s of synaptic activity on blood volume changes. The three curves are for different coupling resistances between the smooth muscle cells, as for Fig. 3.

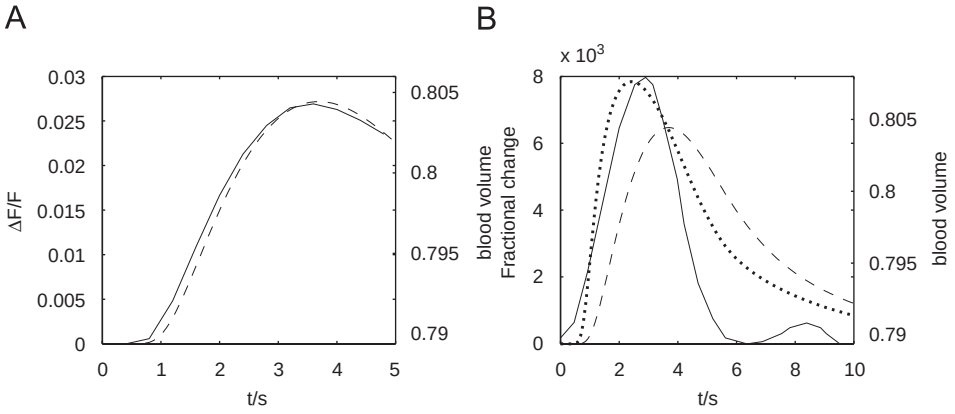

Fig. 6. Comparison between the predictions of the model and experimental results for blood volume changes in arterioles accompanying and following stimulation of local synaptic networks. (A) Solid line, experimental changes in blood volume ($\propto \Delta F/F$) in arterioles during and following stimulation of neural networks in visual area 18 of adult cats with high-contrast vertical and horizontal drifting square gratings for 2 s from zero time (from Figs. 4A in Vanzetta et al., 2005); dashed line, theoretical blood volume calculated using the model. (B) Solid line, experimental changes in blood volume in the microvasculature of the rat barrel cortex in response to stimulation of a single whisker for 2 s (from Fig. 2 in Sheth et al., 2004); dashed line, theoretical blood volume calculated using the model; dotted line, theoretical result with faster muscle kinetics (parameters k_m, k_2, k_3 and k_4 all increased by a multiplicative factor of 10 from their values in Table 1).

by using faster kinetics for the smooth muscle contraction and relaxation, but the theoretical result (dotted line) still shows a slower decline than the experimental one. Various other parameter changes were tried, but the tail of the curve is mainly governed by smooth muscle kinetics once Ca^{2+} is removed, and no one set of parameters will reproduce the correct peak as well as the rapid decline.

4. Discussion

There is now considerable evidence that changes in the BOLD signal in the microcirculation accompanying changes in local electrical activity couple more closely with excitatory synaptic activity than with action potential firing (see, for example, the review by Logothetis, 2002; Sheth et al., 2005). This coupling may be by neurometabolic means, as in the model of Magistretti and Pellerin (1999) (see also Dienel and Cruz, 2003; Aubert et al., 2007), or by neurovascular means (Leybaert, 2005), as in the present model. Favouring the relative importance of the neurovascular model is that the hemodynamic response is driven by neurotransmitter-related signalling and not directly by local energy needs, which are principally driven by action potential firing and postsynaptic currents rather than by presynaptic release of glutamate and the activity of astrocytes (Attwell and Iadecola, 2002). Synaptically released glutamate (Otis et al., 2004; Brasnjo and Otis, 2001) acts on astrocyte metabotropic glutamate receptors (with dissociation constants between 1.2 and 2.6 μM; Martin et al., 1998; Albasanz et al., 1997), giving rise to a second messenger cascade that triggers the release of calcium from internal stores (Cornell-Bell et al., 1990).

EETs are cytochrome P450 metabolites of arachidonic acid and are synthesized in astrocytes from arachidonic acid derived through the actions of calcium on phospholipase A2 and from diacylglycerol, either of which are

stimulated by the action of glutamate on metabotropic receptors in elevating the PIP_2/PLC pathway (Alkayed et al., 1996a,b, 1997; Harder et al., 1998). The resulting increase in calcium can activate phospholipase A2 to convert phospholipids to arachidonic acid which then gives rise to EETs by way of cytochrome P458 (Campbell and Gauthier, 2002). Subsequently, the EETs may be taken up into smooth muscle and metabolized to dihydroxeicosatricenoic acid (DHET) by soluble epoxide hydrolase (Van-Rollins et al., 1996; Fang et al., 2001). The release from astrocytes of EETs allows for their diffusion to effect hyperpolarization of smooth muscle cells of adjacent arterioles (Huang et al., 2005). Evidence that EETs play an important role in blood volume changes in the microcapillary module is provided by the fact that inhibition of EETs substantially decreased changes in regional cerebral blood flow (rCBF) in somatosensory cortex in response to whisker stimulation (Peng et al., 2002) as it does changes in response to rCBF changes due to excitation of NMDA receptors (Bhardwaj et al., 2000). We have therefore allowed for EETs to act as coupling agents between capillaries and arterioles in our model. It should be emphasized, however, that we have no way at present of distinguishing, on the basis of Eqs. (12) and (13), between the present model and one in which the transfer function is between astrocyte calcium and the smooth muscle membrane potential with K^+ acting as an intermediary (see Filosa et al., 2006) or in which a cycloxygenase product acts as an intermediary (see Takano et al., 2006; Zonta et al., 2003). Furthermore, we have not incorporated into the model the fact that EETs can promote the opening of KCa channels in astrocytes (see Gebremedhin et al., 2003; Yamaura et al., 2006).

Finally, the possibility that another factor besides EETs might be involved in astrocyte-smooth muscle coupling (see below) must be entertained, especially as EETs synthesis inhibitors and antagonists apparently do not affect the intitial rise of cerebral blood flow, as measured using a laser-Doppler flow probe, at the barrel cortex surface following whisker stimulation (Shi et al., 2007).

The question arises as to whether there is physiological evidence to support a role for NO in blood volume changes in the microcapillary modules. NO release occurs on stimulating the endothelium of rat middle cerebral arteries but less so on stimulating these cells in third order branches or penetrating arterioles (You et al., 1999; Horiuchi et al., 2003). The increase in rCBF that accompanies rat whisker deflection has been attributed primarily to activation of neuronal NO synthase and not to endothelium NO synthase (Lindauer et al., 1999). Thus there is no change in the rCBF in endothelial NO synthase knockout mice following whisker deflections (Ayata et al., 1996) and no indication of a contribution of endothelial NO synthase in neuronal NO synthase knockout mice in response to whisker deflections (Ma et al., 1996). In humans there is no evidence for a role of NO during regional frontal cortex activation, since blocking both neuronal and endothelial NO synthase does not affect rCBF (White et al., 1999).

Adenosine potentially has a role in coupling excited astrocytes to changes in blood flow. ATP is released both at junctions between astrocytes (Bennett et al., 2005b) as well as being a co-transmitter at neuronal synapses. Ecto-ATPases are found co-localized with sites of ATP release from astrocytes (Joseph et al., 2003) and 5′-ectonucleotidease is also found localized with astrocytes (Braun et al., 1998). Thus the enzymes for converting ATP to adenosine are strategically placed to drive this metabolism at astrocytes. The adenosine A_{2B} receptor type is found in high density at astrocyte endfeet on vascular smooth muscle (Koehler et al., 2006). The conversion of ATP to AMP and then to adenosine by ectoATPase and then ecto-5′-nucleotidase occurs with similar Michaelis–Menten parameter K_m ($\sim$15 μM) to give adenosine concentrations in the brain of the order of 100 nM (Latini and Pedata, 2001; Phillis, 2004). Blocking adenosine receptors in rat barrel cortex significantly attenuates rCBF changes following whisker stimulation (Dirnagl et al., 1994), probably through the A2B receptor subtype (Shi et al., 2007). We have not incorporated adenosine as a potential coupling agent in our model at this stage.

EETs at the astrocyte–arteriole interface initiate a series of events that leads to vasodilation, and thus an increase in blood flow and blood volume in the arteriole. In our model, this is caused by EETs acting on IK_{Ca} and IK_{ATP} channels of smooth muscle cells at the interface to affect a hyperpolarization of these cells. EETs hyperpolarize vascular smooth muscle cells following activation of potassium channels, thus closing voltage-dependent L-type calcium channels and decreasing internal calcium concentration, resulting in vasodilation (Harder et al., 1998; Fleishman et al., 1994; Bennett et al., 2005a). It is known that EETs increase the open-state probability of calcium-activated potassium channels in the vascular smooth muscle cells (Campbell et al., 1996). The net result is to both hyperpolarize the vascular smooth muscle cells, so turning off voltage-dependent calcium channels, as well as directly closing L-type calcium channels (Chen et al., 1999), thus decreasing calcium influx and leading to relaxation and vasodilation. The hyperpolarization produced in the arteriolar smooth muscle cells propagates electrotonically along the muscle cells of the arteriole for up to 3 mm, with 11 mV hyperpolarization giving at least a 16 μm dilation (Emerson and Segal, 2001). There is some evidence that the decay of hyperpolarization from the site of its initiation is not purely electrotonic (see Emerson et al., 2002) but we have not included this effect. It has recently been shown that the photo-release of IP_3 within individual astrocytes results in a highly localized vasodilation of adjacent arterioles in cortical brain slices (Straub et al., 2006). In the present model, such localized dilation can occur if there is moderate to high resistance coupling between the arteriolar smooth muscle cells (Figs. 3 and 4, solid and dashed lines).

Recently, there have been a number of studies that consider direct control of the arteriolar smooth muscle cells by the endfeet of astrocytes impinging on them. Vanzetta et al. (2005) have shown that blood volume changes are first detected at the arteriolar level, with these then spreading to the capillaries and venules, an observation that is consistent with the principal action of astrocytes being on the smooth muscle of the arterioles (but see (Sheth et al., 2005) who suggest that cerebral blood volume changes propagate retrogradely into feeding arterioles). High resolution optical imaging at illuminations between 600–630 nm are sensitive to the oxygen changes in the capillary bed (Frostig et al., 1990) and show that this leads changes in blood volume after an interval of about 700 ms (see Fig. 1D in Vanzetta et al., 2004). Peak values are reached in 2.8–3.5 s, with subsequent decline to 50% of the peak value in 2.5–5 s (Vanzetta et al., 2005; Sheth et al., 2004, 2005). We obtained results for similar changes in arteriolar blood volume. Recently, it has been shown that in the barrel cortex of adult mice a 3 s time lag occurrs between the onset of local field potentials and the beginnings of increases in astrocyte calcium (Wang et al., 2006). This is not compatible with our theoretical predictions (see Fig. 6B), nor apparently with the experimental results of Sheth et al. (2004) on the barrel cortex which show less that 1 s delay between the beginnings of stimulation of a whisker and the beginning of blood-volume changes.

Studies on the direct control of arteriolar smooth muscle by astrocytes have led to apparently conflicting reports. On the one hand, Zonta et al. (2003) have observed vasodilation upon stimulation of glutamate excitatory transmission and upon direct stimulation of astrocytes impinging on the arteriole. On the other hand, it is claimed that Ca^{2+} waves in astrocytes lead to the release of arachidonic acid from their endfeet onto the arteriolar smooth muscle, generating 20-hydroxyeicosatetraenoic acid, giving rise to contraction and vasoconstriction (Mulligan and MacVicar, 2004). It has recently been shown that cyclooxygenase-1 (COX1) metabolites are released from astrocyte endfeet on vascular smooth muscle cells and exert a major vasodilator effect in vivo (Takano et al., 2006). When these observation are confirmed the mechanisms responsible for them can be incorporated into the model presented here.

Acknowledgements

This work was supported by ARC (Australia Research Council) Grant DP0559268.

References

Albasanz, J.L., Ros, M., Martin, M., 1997. Characterization of metabotropic glutamate receptors in rat C6 glioma cells. Eur. J. Pharmacol. 326 (1), 85–91.

Alkayed, N.J., Birks, E.K., Hudetz, A.G., Roman, R.J., Henderson, L., Harder, D.R., 1996a. Inhibition of brain P-450 arachidonic acid epoxygenase decreases baseline cerebral blood flow. Am. J. Physiol. 271, H1541–H1546.

Alkayed, N.J., Narayanan, J., Gebremedhin, D., Medhora, M., Roman, R.J., Harder, D.R., 1996b. Molecular characterization of an arachidonic acid epoxygenase in rat brain astrocytes. Stroke 27 (5), 971–979.

Alkayed, N.J., Birks, E.K., Narayanan, J., Petrie, K.A., Kohler-Cabot, A.E., Harder, D.R., 1997. Role of P-450 arachidonic acid epoxygenase in the response of cerebral blood flow to glutamate in rats. Stroke 28, 1066–1072.

Anderson, C.M., Nedergaard, M., 2003. Astrocyte-mediated control of cerebral microcirculation. Trends Neurosci. 26 (7), 340–344.

Attwell, D., Iadecola, C., 2002. The neural basis of functional brain imaging signals. Trends Neurosci. 25 (12), 621–625.

Aubert, A., Costalat, R., 2002. A model of the coupling between brain electrical activity, metabolism, and hemodynamics: application to the interpretation of functional neuroimaging. Neuroimage 17 (3), 1162–1181.

Aubert, A., Pellerin, L., Magistretti, P.J., Costalat, R., 2007. A coherent neurobiological framework for functional neuroimaging provided by a model integrating compartmentalized energy metabolism. Proc. Natl Acad. Sci. USA 104, 4188–4193.

Ayata, C., Ma, J., Meng, W., Huang, P., Moskowitz, M.A., 1996. L-NA-sensitive rCBF augmentation during vibrissal stimulation in synthase mutant mice. J. Cerebral Blood Flow Metabolism 16, 539–541.

Bennett, M.R., 1972. Autonomic Neuromuscular Transmission. Monographs of the Physiological Society. Cambridge University Press, Cambridge.

Bennett, M.R., Farnell, L., Gibson, W.G., Lin, Y.Q., Blair, D.H., 2001. Quantal and non-quantal current and potential fields around individual sympathetic varicosities on release of ATP. Biophys. J. 80, 1311–1328.

Bennett, M.R., Farnell, L., Gibson, W.G., 2005a. A quantitative description of the contraction of blood vessels following the release of noradrenaline from sympathetic varicosities. J. Theoret. Biol. 234, 107–122.

Bennett, M.R., Farnell, L., Gibson, W.G., 2005b. A quantitative model of purinergic junctional transmission of calcium waves in astrocyte networks. Biophys. J. 89 (4), 2235–2250.

Bennett, M.R., Buljan, V., Farnell, L., Gibson, W.G., 2006. Purinergic junctional transmission and propagation of calcium waves in spinal cord astrocyte networks. Biophys. J. 91, 3560–3571.

Bhardwaj, A., Northington, F.J., Carhuapoma, J.R., Falck, J.R., Harder, D.R., Traystman, R.J., Koehler, R.C., 2000. P-450 epoxygenase and NO synthase inhibitors reduce cerebral blood flow response to N-methyl-D-aspartate. Am. J. Physiol.—Heart Circulatory Physiol. 279 (4), H1616–H1624.

Brasnjo, G., Otis, T.S., 2001. Neuronal glutamate transporters control activation of postsynaptic metabotropic glutamate receptors and influence cerebellar long-term depression. Neuron 31 (4), 607–616.

Braun, N., Zhu, Y., Krieglstein, J., Culmsee, C., Zimmermann, H., 1998. Upregulation of the enzyme chain hydrolyzing extracellular ATP after transient forebrain ischemia in the rat. J. Neurosci. 18 (13), 4891–4900.

Buxton, R.B., Frank, L.R., 1997. A model for the coupling between cerebral blood flow and oxygen metabolism during neural stimulation. J. Cerebral Blood Flow Metabolism 17 (1), 64–72.

Buxton, R.B., Wong, E.C., Frank, L.R., 1998. Dynamics of blood flow and oxygenation changes during brain activation: the balloon model. Magn. Resonance Med. 39 (6), 855–864.

Campbell, W.B., Gauthier, K.M., 2002. What is new in endothelium-derived hyperpolarizing factors? Curr. Opin. Nephrol. Hypertension 11 (2), 177–183.

Campbell, W.B., Gebremedhin, D., Pratt, P.F., Harder, D.R., 1996. Identification of epoxyeicosatrienoic acids as endothelium-derived hyperpolarizing factors. Circulation Res. 78 (3), 415–423.

Chen, J., Capdevila, J.H., Zeldin, D.C., Rosenberg, R.L., 1999. Inhibition of cardiac L-type calcium channels by epoxyeicosatrienoic acids. Mole. Pharmacol. 55, 288–295.

Cornell-Bell, A.H., Finkbeiner, S.M., Cooper, M.S., Smith, S.J., 1990. Glutamate induces calcium waves in cultured astrocytes: long-range glial signaling. Science 247 (4941), 470–473.

Dani, J.W., Chernjavsky, A., Smith, S.J., 1992. Neuronal activity triggers calcium waves in hippocampal astrocyte networks. Neuron 8 (3), 429–440.

De Young, G.W., Keizer, J., 1992. A single-pool inositol 1,4,5-trisphosphate-receptor-bases model for agonsit-stimulated oscillations in Ca2+ concentration. Proc. Natl Acad. Sci. USA 89, 9895–9899.

Devor, A., Ulbert, I., Dunn, A.K., Narayanan, S.N., Jones, S.R., Anderman, M.L., Boas, D.A., Dale, A.M., 2005. Coupling of the cortical hemodynamic response to cortical and thalamic neuronal activity. Proc. Natl Acad. USA 102, 3822–3827.

Dienel, G.A., Cruz, N.F., 2003. Neighborly interactions of metabolically-activated astrocytes in vivo. Neurochem. Int. 43 (4–5), 339–354.

Dirnagl, U., Niwa, K., Lindauer, U., Villringer, A., 1994. Coupling of cerebral blood flow to neuronal activation: role of adenosine and nitric oxide. Am. J. Physiol. 267 (1 Pt 2), H296–H301.

Emerson, G.G., Segal, S.S., 2001. Electrical activation of endothelium evokes vasodilation and hyperpolarization along hamster feed arteries. Am. J. Physiol.—Heart Circulatory Physiol. 280 (1), H160–H167.

Emerson, G.G., Neild, T.O., Segal, S.S., 2002. Conduction of hyperpolarization along hamster feed arteries: augmentation by acetylcholine. Am. J. Physiol.—Heart Circulatory Physiol. 283, 102–109.

Fang, X., Kaduce, T.L., Weintraub, N.L., Harmon, S., Teesch, L.M., Morisseau, C., Thompson, D.A., Hammock, B.D., Spector, A.A., 2001. Pathways of epoxyeicosatrienoic acid metabolism in endothelial cells. implications for the vascular effects of soluble epoxide hydrolase inhibition. J. Biol. Chem. 276 (18), 14867–14874.

Filosa, J.A., Bonev, A.D., Nelson, M.T., 2004. Calcium dynamics in cortical astrocytes and arterioles during neurovascular coupling. Circulation Res. 95, e73–e81.

Filosa, J.A., Bonev, A.D., Straub, S.V., Meredith, A.L., Wilkerson, M.K., Aldrich, R.W., Nelson, M.T., 2006. Local potassium signaling couples neuronal activity to vasodilation in the brain. Nature Neurosci. 9, 1397–1403.

Fink, C.F., Schlepenko, B., Loew, L.M., 1999. Determination of time-dependent inositol-1,4,5-trisphosphate concentration during calcium release in a smooth muscle cell. Biophys. J. 77, 617–628.

Fleishman, B.K., Murray, R.K., Kotlikoff, M.I., 1994. Voltage window for sustained elevation of cytosolic calcium in smooth muscle cells. Proc. Natl Acad. Sci. USA 91, 11914–11918.

Frostig, R.D., Lieke, E.E., Ts'o, D.Y., Grinvald, A., 1990. Cortical functional architecture and local coupling between neuronal activity and the microcirculation revealed by in vivo high-resolution optical imaging of intrinsic signals. Proc. Natl Acad. Sci. USA 87 (16), 6082–6086.

Gebremedhin, D., Yamaura, K., Zhang, C., Bylund, J., Koehler, R.C., Harder, D.R., 2003. Metabotropic glutamate receptor activation enhances the activities of two types of Ca^{2+}-activated K^+ channels in rat hippocampal astrocytes. J. Neurosci. 23, 1678–1687.

Hai, C.-M., Murphy, R.A., 1988. Regulation of shortening velocity by cross-bridge phosphorylation in smooth muscle. Am. J. Physiol.—Cell Physiology 255, C86–C94.

Harder, D.R., Alkayed, N.J., Lange, A.R., Gebremedhin, D., Roman, R.J., 1998. Functional hyperemia in the brain: hypothesis for astrocyte-derived vasodilator metabolites. Stroke 29 (1), 229–234.

Harder, D.R., Roman, R.J., Gebremedhin, D., 2000. Molecular mechanisms controlling nutritive blood flow: role of cytochrome p450 enzymes. Acta Physiol. Scand. 168, 543–549.

Harrison, R.V., Harel, N., Panesar, J., Mount, R.J., 2002. Blood capillary distribution correlates with hemodynamic-based functional imaging in cerebral cortex. Cerebral Cortex 12 (3), 225–233.

Haydon, P.G., Carmignoto, G., 2006. Astrocyte control of synaptic transmission and neurovascular coupling. Physiol. Rev. 86, 1009–1031.

Hoge, R.D., Atkinson, J., Gill, B., Crelier, G.R., Marrett, S., Pike, G.B., 1999. Linear coupling between cerebral blood flow and oxygen consumption in activated human cortex. Proc. Natl Acad. Sci. USA 96 (16), 9403–9408.

Horiuchi, T., Dietrich, H.H., Hongo, K., Jr, R.G.D., 2003. Comparison of P2 receptor subtypes producing dilation in rat intracerebral arterioles. Stroke 34 (6), 1473–1478.

Huang, A., Sun, D., Jacobson, A., Carroll, M.A., Falck, J.R., Kaley, G., 2005. Epoxyeicosatrienoic acids are released to mediate shear stress-dependent hyperpolarization of arteriolar smooth muscle. Circulation Res. 96 (3), 376–383.

Jones, M., Berwick, J., Johnston, D., Mayhew, J., 2001. Concurrent optical imaging spectroscopy and laser-doppler flowmetry: the relationship between blood flow, oxygenation, and volume in rodent barrel cortex. Neuroimage 13 (6 Pt 1), 1002–1015.

Joseph, S.M., Buchakjian, M.R., Dubyak, G.R., 2003. Colocalization of ATP release sites and ecto-ATPase activity at the extracellular surface of human astrocytes. J. Biol. Chem. 278 (26), 23331–23342.

Koehler, R.C., Gebremedhin, D., Harder, D.R., 2006. Role of astrocytes in cerebrovascular regulation. J. Appl. Physiol. 100 (1), 307–317.

Latini, S., Pedata, F., 2001. Adenosine in the central nervous system: release mechanisms and extracellular concentrations. J. Neurochem. 79 (3), 463–484.

Lemon, G., Gibson, W.G., Bennett, M.R., 2003. Metabotropic receptor activation, desensitization and sequestration-I: modelling calcium and inositol 1,4,5-trisphosphate dynamics following receptor activation. J. Theoret. Biol. 223 (1), 93–111.

Leybaert, L., 2005. Neurobarrier coupling in the brain: a partner of neurovascular and neurometabolic coupling? J. Cerebral Blood Flow Metabolism 25 (1), 2–16.

Li, Y.-X., Rinzel, J., 1994. Equations for InsP3 receptor-mediated [Ca2+] oscillations derived from a detailed kinetic model: a Hodgkin-Huxley like formalism. J. Theoret. Biol. 166, 461–473.

Lindauer, U., Megow, D., Matsuda, H., Dirnagl, U., 1999. Nitric oxide: a modulator, but not a mediator, of neurovascular coupling in rat somatosensory cortex. Am. J. Physiol. 277 (2 Pt 2), H799–H811.

Logothetis, N.K., 2002. The neural basis of the blood-oxygen-level-dependent functional magnetic resonance imaging signal. Phil. Trans. R. Soc. London—Ser. B: Biol. Sci. 357 (1424), 1003–1037.

Ma, J., Ayata, C., Huang, P.L., Fishman, M.C., Moskowitz, M.A., 1996. Regional cerebral blood flow response to vibrissal stimulation in mice lacking type i nos gene expression. Am. J. Physiol. 270 (3 Pt 2), H1085–H1090.

Magistretti, P., Pellerin, L., 1996. Cellular basis of brain energy metabolism and their relevance to functional brain imaging: evidence for a prominent role of astrocytes. Cerebral Cortex 6 (1), 50–61.

Magistretti, P., Pellerin, L., 1999. Astrocytes couple synaptic activity to glucose utilization in the brain. News Physiol. Sci. 14, 177–182.

Malonek, D., Grinvald, A., 1996. Interactions between electrical activity and cortical microcirculation revealed by imaging spectroscopy: implications for functional brain mapping. Science 272, 551–554.

Malonek, D., Dirnagl, U., Lindauer, U., Yamada, K., Kanno, I., Grinvald, A., 1997. Vascular imprints of neuronal activity: relationships between the dynamics of cortical blood flow, oxygenation, and volume changes following sensory stimulation. Proc. Natl Acad. Sci. USA 94, 14826–14831.

Martin, M., Albasanz, J.L., Fernandez, M., Ros, M., 1998. Cross-talk between beta-adrenergic and metabotropic glutamate receptors in rat C6 glioma cells. Biochim. Biophys. Acta 1393 (1), 186–192.

Mulligan, S.J., MacVicar, B.A., 2004. Calcium transients in astrocyte endfeet cause cerebrovascular constrictions. Nature 431 (7005), 195–199.

Nemoto, M., Sheth, S., Guiou, M., Pouratian, N., Chen, J.W., Toga, A.W., 2004. Functional signal- and paradigm-dependent linear relationships between synaptic activity and hemodynamic responses in rat somatosensory cortex. J. Neurosci. 24 (15), 3850–3861.

Otis, T.S., Brasnjo, G., Dzubay, J.A., Pratap, M., 2004. Interactions between glutamate transporters and metabotropic glutamate receptors at excitatory synapses in the cerebellar cortex. Neurochem. Int. 45 (4), 537–544.

Peng, X., Carhuapoma, J.R., Bhardwaj, A., Alkayed, N.J., Falck, J.R., Harder, D.R., Traystman, R.J., Koehler, R.C., 2002. Suppression of cortical functional hyperemia to vibrissal stimulation in the rat by epoxygenase inhibitors. Am. J. Physiol.—Heart Circulatory Physiol. 283 (5), H2029–H2037.

Phillis, J.W., 2004. Adenosine and adenine nucleotides as regulators of cerebral blood flow: roles of acidosis, cell swelling, and KATP channels. Crit. Rev. Neurobiol. 16 (4), 237–270.

Ramón y Cajal, S., 1995. Histological Nervous System, vol. 1. Oxford University Press, New York.

Rubart, M., Patlak, J.B., Nelson, M.T., 1996. Ca2+ currents in cerebral artery smooth muscle cells of rat at physiological Ca2+ concentrations. J. General Physiol. 107, 459–472.

Seidel, M.F., Simard, J.M., Hunter, S.F., Campbell, G.A., 1991. Isolation of arteriolar microvessels and culture of smooth muscle cells from cerebral cortex of guinea pig. Cell Tissue Res. 265, 579–587.

Sheth, S.A., Nemoto, M., Guiou, M., Walker, M., Pouratian, N., Hageman, N., Toga, A.W., 2004. Columnar specificity of microvascular oxygenation and volume responses: implications for functional brain mapping. Journal of Neuroscience 24 (3), 634–641.

Sheth, S.A., Nemoto, M., Guiou, M.W., Walker, M.A., Toga, A.W., 2005. Spatiotemporal evolution of functional hemodynamic changes and their relationship to neuronal activity. J. Cerebral Blood Flow Metabolism 25 (7), 830–841.

Shi, Y., Liu, X., Gebremedhin, D., Falck, J.R., Harder, D.R., Koehler, R.C., 2007. Interactions of mechanisms involving epoxyeicosatrienoic acids, adenosine receptors, and metabotropic glutamate receptors in neurovascular coupling in rat whisker barrel cortex. J. Cerebral Blood Flow Metabolism, doi:10:1038/sj.jcbfm.9600511.

Straub, S.V., Bonev, A.D., Wilkerson, M.K., Nelson, M.T., 2006. Dynamic inositol trisphosphate-mediated calcium signals within astrocytic endfeet underlie vasodilation of cerebral arterioles. J. General Physiol. 128 (6), 659–669.

Takano, T., Tian, G.F., Peng, W., Lou, N., Libionka, W., Han, X., Nedergaard, M., 2006. Astrocyte-mediated control of cerebral blood flow. Nature Neurosci. 9 (2), 260–267.

Tyml, K., Anderson, D., Lidington, D., Ladak, H.M., 2003. A new method for assessing arteriolar diameter and hemodynamic resistance using image analysis of vessel lumen. Am. J. Physiol.—Heart Circulatory Physiol. 284 (5), H1721–H1728.

VanRollins, M., Kaduce, T.L., Fang, X., Knapp, H.R., Spector, A.A., 1996. Arachidonic acid diols produced by cytochrome P-450 monooxygenases are incorporated into phospholipids of vascular endothelial cells. J. Biol. Chem. 271 (24), 14001–14009.

Vanzetta, I., Slovin, H., Omer, D.B., Grinvald, A., 2004. Columnar resolution of blood volume and oximetry functional maps in the behaving monkey; implications for FMRI. Neuron 42 (5), 843–854.

Vanzetta, I., Hildesheim, R., Grinvald, A., 2005. Compartment-resolved imaging of activity-dependent dynamics of cortical blood volume and oximetry. J. Neurosci. 25 (9), 2233–2244.

Wang, X., Lou, N., Xu, Q., Tian, G.-F., Peng, W.G., Han, X., Kang, J., Takano, T., Nedergaard, M., 2006. Astrocytic Ca^{2+} signalling evoked by sensory stimulation *in vivo*. Nature Neurosci. 9, 816–823.

White, R.P., Hindley, C., Bloomfield, P.M., Cunningham, V.J., Vallance, P., Brooks, D.J., Markus, H.S., Wu, X., Haystead, T.A., Nakamoto, R.K., Somlyo, A.V., Somlyo, A.P., 1999. The effect of the nitric oxide synthase inhibitor L-NMMA on basal CBF and vasoneuronal coupling in man: a PET study. J. Cerebral Blood Flow Metabolism 19 (6), 673–678.

Yamaura, K., Gebremedhin, D., Zhang, C., Narayanam, J., Hoefert, K., Jacobs, E.R., Koehler, R.C., Harder, D.R., 2006. Contributions of epoxyeicosatrienoic acids to the hypoxia-induced activation of Ca^{2+}-activated K^+ channels in cultured rat hippocampal astrocytes. Neuroscience 143, 703–716.

You, J., Johnson, T.D., Marrelli, S.P., Bryan, R.M., 1999. Functional heterogeneity of endothelial P2 purinoceptors in the cerebrovascular tree of the rat. Am. J. Physiol. 277 (3 Pt 2), H893–H900.

Zheng, Y., Martindale, J., Johnston, D., Jones, M., Berwick, J., Mayhew, J., 2002. A model of the hemodynamic response and oxygen delivery to brain. Neuroimage 16 (3 Pt 1), 617–637.

Zonta, M., Angulo, M.C., Gobbo, S., Rosengarten, B., Hossmann, K.-A., Pozzan, T., Carmignoto, G., 2003. Neuron-to-astrocyte signaling is central to the dynamic control of brain microcirculation. Nature Neurosci. 6 (1), 43–50.